Inorganic Chemistry

Article

pubs.acs.org/IC

Metal-to-Ligand Charge-Transfer Emissions of Ruthenium(II) Pentaammine Complexes with Monodentate Aromatic Acceptor Ligands and Distortion Patterns of their Lowest Energy Triplet Excited States

Chia Nung Tsai,[†] Shivnath Mazumder,[‡] Xiu Zhu Zhang,[†] H. Bernhard Schlegel,*[,‡] Yuan Jang Chen,*[,†] and John F. Endicott*[,‡]

[†]Department of Chemistry, Fu-Jen Catholic University, New Taipei City 24205, Taiwan, R.O.C.

[‡]Department of Chemistry, Wayne State University, Detroit, Michigan 48202, United States

Supporting Information

ABSTRACT: This is the first report of the 77 K triplet metal-to-ligand charge-transfer (^{3}MLCT) emission spectra of pentaammine−MDA−ruthenium(II) ($[Ru(NH_3)_5(MDA)]^{2+}$) complexes, where MDA is a monodentate aromatic ligand. The emission spectra of these complexes and of the related *trans*-$[Ru(NH_3)_4(MDA)\ (MDA')]^{2+}$ complexes are closely related, and their emission intensities are very weak. Density functional theory (DFT) calculations indicate that the energies of the lowest ^{3}MLCT excited states of Ru−MDA complexes are either similar to or lower than those of the lowest energy metal-centered excited states ($^3MC_{X(Y)}$), that the barrier to internal conversion at 77 K is large compared to k_BT, and that the $^3MC_{X(Y)}$ excited states are weakly bound. The $[Ru(NH_3)_5py]^{2+}$ complex is an exception to the general pattern: emission has been observed for the $[Ru(ND_3)_5(d_5\text{-py})]^{2+}$ complex, but its lifetime is apparently very short. DFT modeling indicates that the excited state distortions of the different ^{3}MC excited states are very large and are in both Ru−ligand bonds along a single Cartesian axis for each different ^{3}MC excited state, nominally resulting in $^3MC_{X(Y)}$, $^3MC_{(X)Y}$, and ^3MC_Z lowest energy metal-centered states. The $^3MC_{X(Y)}$ and $^3MC_{(X)Y}$ states appear to be the pseudo-Jahn−Teller distorted components of a $^3MC_{(XY)}$ state. The $^3MC_{X(Y)}$ states are distorted up to 0.5 Å in each H_3N−Ru−NH_3 bond along a single Cartesian axis in the pentaammine and *trans*-tetraammine complexes, whereas the ^3MC_Z states are found to be dissociative. DFT modeling of the ^{3}MLCT excited state of $[Ru(NH_3)_5(py)]^{2+}$ indicates that the Ru center has a spin density of 1.24 at the ^{3}MLCT energy minimum and that the ^{3}MLCT → ^3MC_Z crossing is smooth with a very small barrier (<0.5 kcal/mol) along the D_3N−Ru−py distortion coordinate, implying strong ^{3}MLCT/^{3}MC excited state configurational mixing. Furthermore, the DFT modeling indicates that the long-lived intermediate observed in earlier flash photolysis studies of $[Ru(NH_3)_5py]^{2+}$ is a Ru^{II}-(η^2(C═C)-py) species.

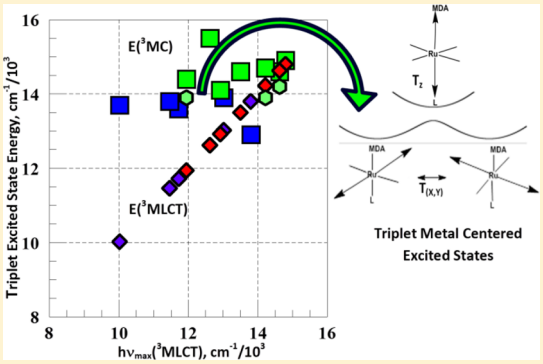

INTRODUCTION

In order to design photosensitizers in a rational manner, it is necessary to determine the molecular properties that will optimize the efficiencies of the desired photoinduced chemical reaction. In order to efficiently promote the electron transfer from (or to) the sensitizer's excited state, the efficiencies of competing excited state decay pathways must be minimized. These competing decay pathways determine the intrinsic lifetimes of the complexes and have been extensively studied from a variety of perspectives.[1−15] The characterization of the lowest energy excited states of transition metal complexes is particularly challenging due to (a) the presence of several excited states that differ little in energy and (b) the role of spin orbit coupling in promoting mixing between states of different spin multiplicities. These issues are of considerable importance in [ruthenium(II)−(aromatic ligand)] (Ru−A) based photosensitizers. If only because of the complexity of evaluating the consequences of the interactions between low-energy electronic states, then it is necessary to examine the excited state properties of complexes in which the ordering and even the kind of excited states in the low-energy regime are altered by variations of the ancillary ligands and/or the acceptor ligand. The pentaammine−ruthenium(II) complexes with monodentate aromatic ligand acceptors ($[Ru^{II}(NH_3)_5(MDA)]^{2+}$) such as pyridine (py), which contain a single aromatic ring, represent one kind of limit for Ru−A complexes since (a) the ancillary ligands form simple σ-bonds to Ru^{II} that should not contribute significantly to the electronic configurations of metal-to-ligand charge-transfer (MLCT) excited states and their bond length

Received: May 26, 2015
Published: August 24, 2015

DOI: 10.1021/acs.inorgchem.5b01193
Inorg. Chem. 2015, 54, 8495−8508

distortions are not restricted by ligand stereochemistry and (b) the MDA acceptor LUMOs can have relatively high energies so that the MLCT excited states of Ru−MDA chromophores might also be expected at relatively high energies. Thus, such complexes should approximate the ideal limit of Ru−complex excited state properties, which have molecular and electronic structures that are characteristic of each electronic state unaltered by intra- and interligand stereochemical constraints. However, prior to the present work, there has been no report of emission from these complexes, and the $[Ru^{II}(NH_3)_5(py)]^{2+}$ prototype of the series has been not only alleged not to emit but also its room temperature irradiation leads to a relatively long-lived chemical intermediate that decays, at least partly, to regenerate the ground state chromophore.[14,16,17]

We have recently been using a combination of spectroscopic and computational modeling studies to characterize triplet excited state manifolds of ruthenium chromophores.[18−21] Prior to the present report, this work has found that the ^{3}MLCT excited states are relatively well-bound and that the ^{3}MC excited states are much more distorted and often only weakly bound. Thus, we have found that at least some $[Ru(NH_3)_4(MDA)(MDA')]^{2+}$ complexes have weak visible region emissions in 77 K glasses, but the weakness of these emissions appears to be a result of their very small emission quantum yields (ϕ_{em}) rather than unusually short lifetimes that might be attributed to fast internal conversion (IC) from the ^{3}MLCT to a ^{3}MC excited state.[19]

Evaluation of the role of near-in-energy ^{3}MC excited states in altering the properties of the lowest energy ^{3}MLCT excited states of Ru^{II}−A chromophores has been difficult since their ^{3}MC emissions have not been reported even though electronically related metal-centered emissions are well-known for many complexes of trivalent metals with nd^6 (and nd^3) electronic configurations.[14,22] Hauser and co-workers have recently concisely summarized the problems and literature related to the characterization of Ru^{II} ^{3}MC states.[23] As these authors note, the only experimental observations that relate to the role of ^{3}MC states are based on the time difference between ^{3}MLCT absorption decay and ground state absorption recovery, complemented by density functional theory (DFT) calculations to demonstrate that ^{3}MLCT and ^{3}MC excited states are near in energy, that IC can greatly alter ^{3}MLCT lifetimes, and that the relative energies of these excited states can be stereochemically manipulated for some $[Ru(PP)_3]^{2+}$, where PP = bipyridine (bpy) or a methyl-substituted bipyridine.[15] We have approached this problem using DFT modeling[18−21] of the triplet excited states in combination with emission spectroscopic observations. We use a contemporary version of Gaussian[24] that incorporates the Franck−Condon approximation, as developed by Barone and co-workers.[13,25−28] This approach has allowed us to construct models of the distorted Ru−bpy ^{3}MLCT excited states that are consistent with the inferences from resonance-Raman spectra and that reproduce the variations in the vibronic side band of their emission spectra very well,[18,20] and we have recently been applying these approaches to the modeling of ^{3}MC excited states of complexes with Ru−A chromophores.[19−21,29] This work has found very large differences in the Ru−ligand distortions for ^{3}MLCT and ^{3}MC excited states, which can lead to large reorganizational energies for the IC between them. The resulting reorganizational barriers to IC can be much larger than $4k_BT$ at 77 K when the ^{3}MC state is the lowest energy excited state, resulting in a higher energy local minimum for the ^{3}MLCT excited state and a strong emission from the upper state[20,21] ("non-Kasha" behavior).[30] The DFT modeling of the $[Ru(NH_3)_4(pz)_2]^{2+}$ complex indicated that the ^{3}MLCT and ^{3}MC excited states had comparable energies, and it was postulated that the much smaller quantum yields than those found for Ru−bpy chromophores were a consequence of the efficiency of producing the emitting MLCT excited states, γ, from Ru−MDA Franck−Condon excited states that are initially generated by light absorption.[19] The present article includes additional studies of $[Ru(NH_3)_4(MDA)(MDA')]^{2+}$, as well as the $[Ru^{II}(NH_3)_5(MDA)]^{2+}$ complexes. These complexes span a range of calculated ^{3}MLCT/^{3}MC excited state energy differences and demonstrate that the lowest energy excited state properties of the $[Ru^{II}(NH_3)_5(MDA)]^{2+}$ and $[Ru(NH_3)_4(MDA)(MDA')]^{2+}$ complexes are similar in kind, that their lifetimes and emission quantum yields are independent of the calculated ^{3}MLCT/^{3}MC excited state energy differences, and that it is most likely that $\gamma \approx 1$.

EXPERIMENTAL SECTION

Materials and Synthesis of Compounds. Pyrazine (pz), pyridine (py), 4-acetyl-pyridine (ac-py), 4-phenyl-pyridine (ph-py), 4,4′-bipyridine (4,4′-bpy), 2,2′-bipyridine (bpy), 2,2′-bipyridylammine (bpyam), ferrocene, and trifluoromethanesulfonic acid (HOTf) were purchased from Aldrich, and $[Ru(NH_3)_6]Cl_3$ and NH_4PF_6 were purchased from STREM Chemicals and used without further purification. The syntheses of $[Ru(NH_3)_5Cl]Cl_2$, $[Ru(NH_3)_5(H_2O)](PF_6)_2$, *cis*-$[Ru(NH_3)_4(Cl)_2]Cl$, and *trans*-$[Ru(NH_3)_4(L)(H_2O)](PF_6)_2$,[31,32] L = 4-phenyl-pyridine (ph-py), NH_3, and 4-acetyl-pyridine (ac-py), have been reported previously. Literature syntheses were used for the following compounds: $[Ru(NH_3)_5(L)]^{2+}$ complexes with L = py, ac-py, ph-py, 4,4′-bipyridine (4,4′-bpy), and pyrazine (pz) and[17,33−35] *cis*-/*trans*-$[Ru(NH_3)_4(L)_2](PF_6)_2$ with L = pz, py, ac-py, and ph-py (Figure 1).[36−40] Variations in previously reported syntheses were used for the following compounds: *trans*-$[Ru(NH_3)_4(py)(pz)](PF_6)_2$,[39] *mer*-$[Ru(NH_3)_3(bpy)(L)](PF_6)_2$ (L = py, pz,[19,31] ac-py, CH_3CN[21,41]), *mer*-$[Ru(NH_3)_3(bpyam)(pz)](PF_6)_2$,[19] $[Ru(bpy)(Am)_4](PF_6)_2$ ($(Am)_4$ = $(NH_3)_4$ and $(en)_2$),[42−44] and $[Ru(bpy)_2(NH_3)_2](PF_6)_2$.[45] Am(m)ine deuterated complexes were

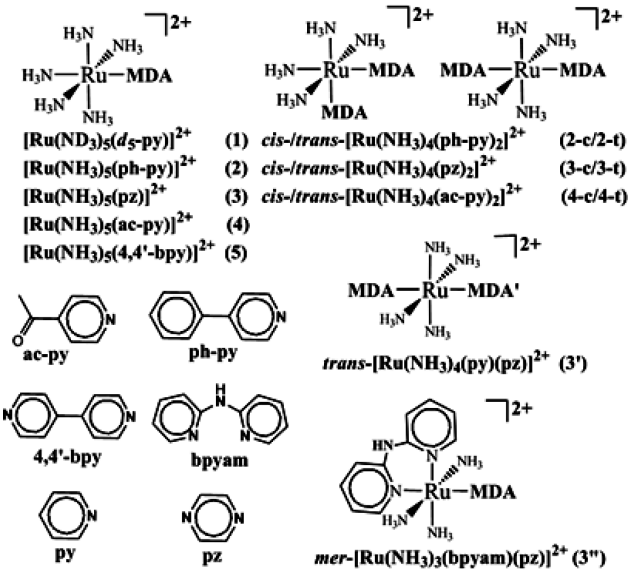

Figure 1. Ru complexes with MDA ligand-based MLCT emissions; the six MDA ligands used are at the lower left. The code numbers are chosen to agree with those in Table 1.

DOI: 10.1021/acs.inorgchem.5b01193
Inorg. Chem. 2015, 54, 8495−8508

prepared by dissolving the corresponding $[Ru(NH_3)_5(MDA)](PF_6)_2$ complex in D_2O and then precipitating it with the addition of saturated $NaPF_6/D_2O$ solution. This procedure was repeated several times as described previously.[46] Complexes were independently synthesized, and their spectra emission spectra were determined two or more times.

Instrumentation. The electrochemical measurements were performed using a BASi Epsilon electrochemical workstation. Cyclic voltammograms (CV) and differential pulse voltammograms (DPV) were obtained in acetonitrile solution, which contained 10^{-3} M complex and 0.1 M *n*-tetrabutylammonium hexafluorophosphate (*n*-TBAH) at scan rates of 100 and 4 mV/s, respectively. A three-electrode system consisting of a Pt-disk (1 mm) as a working electrode, polished with 0.1−0.3 μm Baikowski alumina suspension, a Pt-wire as the counter electrode, and Ag/AgCl as the reference electrode was used. Ferrocene (0.437 V vs Ag/AgCl in acetonitrile) was used as the internal standard.

The 298 K absorption spectra in the solution of CH_3CN were determined with a Shimadzu UV-3101PC spectrophotometer. Absorption spectra in 87 K butyronitrile glasses were obtained as described in detail elsewhere[19,47] using a calibrated Xe line emission lamp for wavelength and an Oriel model 63966 quartz tungsten halogen QTH lamp for intensity. A QTH lamp was also used as the light source in the determination of 87 K absorption spectra for the emission yield measurements. A P/N 21530 Specac variable temperature cell (−190 ∼ 250 °C) with a square 1 cm quartz cuvette was used as the controlled-temperature cell holder with liquid or glass samples. The detection system contained a motor-driven Jobin Yvon H-10 Vis monochromator, a Hamamatsu R928 phototube with a Jobin-Yvon (JY) PMT-HVPS power supply, a JY Spectracq2 for data acquisition, and JY SynerJY software for data acquisition and data analysis.

Emission spectra and lifetimes in 77 K glasses were obtained in 2 mm i.d. cylindrical quartz cells in a spectroscopic quartz dewar as described in detail elsewhere.[19−21,48] Emission spectral wavelengths were calibrated with Xe emission lines for wavelength; intensities were calibrated with an Oriel model 63358 or 63966 quartz tungsten halogen QTH lamp. The emission spectra were collected using slightly different systems (the detector heads of both systems were cooled to −90 °C, and the spectrometers were purged with dry N_2):

(a) An Andor Shamrock 500 spectrometer with dual exit ports equipped with three gratings: 150 l/mm, 800 nm blaze; 600 l/mm, 500 nm blaze; 300 l/mm, 1200 nm blaze. Andor Newton DU920-BV (for the visible range) and Andor iDus-InGaAs DU490A-1.7 (for the NIR) detector heads were mounted on the dual exit ports of a Shamrock 500 spectrometer.

(b) A Horiba Jobin Yvon iHR 550 spectrometer equipped with three gratings (300 l/mm, 600 nm blaze; 300 l/mm, 1 μm blaze; and 600 l/mm, 1 μm blaze). Horiba Symphony InGaAs-1700 (for the NIR) detector head was mounted on the exit port of a iHR 550 spectrometer. This system was operated using SynerJY software.

The 77 K emission lifetimes were determined using a Spectra Physics VSL-337ND-S nitrogen laser-pumped DUO-210 dye laser system or using a LTB model MNL 103-PD nitrogen laser-pumped or a LTB model DUL 100 dye laser system, a Hamamatsu P9220 PMT/E717-63 mounted on a Jobin-Yvon H-100 spectrometer for collection in the visible region or a Hamamatsu NIR-PMT model H10330A-75 for collection in the NIR region, and a National Instruments NI PCI-5154, 2 GS/s, 1 GHz digitizer w/8 MB/ch onboard memory PC card as described previously[18,19,21] or a LeCroy WaveRunner 6030A.

Computational Details. DFT[24] calculations have been performed to compute the triplet PE surfaces of the Ru complexes. The calculations have been done with a development version of Gaussian[24] with the B3PW91 functional[49−51] and SDD basis set and pseudopotential[52] on the metal and 6-31G(d) basis[53,54] on the lighter atoms. Solvation effects (in acetonitrile) were accounted for using the implicit SMD solvation model[55] and were included during structure optimization. Wave functions were tested for SCF stability,[56−59] and all of the optimized structures were confirmed as minima by analyzing the harmonic vibrational frequencies. The ground state singlet and triplet states were computed using the standard SCF method, and analytical frequencies were obtained for each. DFT has an intrinsic problem of determining the accurate relative energies of states having largely different electron densities and distributions;[60,61] nevertheless, it is regarded as being fairly reliable for calculating trends in a series of related complexes.[61] The isodensity plots of the orbitals were visualized using GaussView.[62]

RESULTS

Experimental Results. The $[Ru(NH_3)_5(MDA)]^{2+}$ complexes (MDA = pz, ph-py, ac-py, and 4,4′-bpy) have all been found to emit weakly at 77 K (Figure S1).[41] However, we had to perdeuterate $[Ru(NH_3)_5(py)]^{2+}$ in order to detect its 77 K emission. We collected the 77 K emission spectra from the $[Ru(ND_3)_5(MDA)]^{2+}$ complexes with MDA = pz, ph-py, ac-py, and 4,4′-bpy in an attempt to resolve some vibronic side band structure, but none was resolved, as shown in Figure 2. This

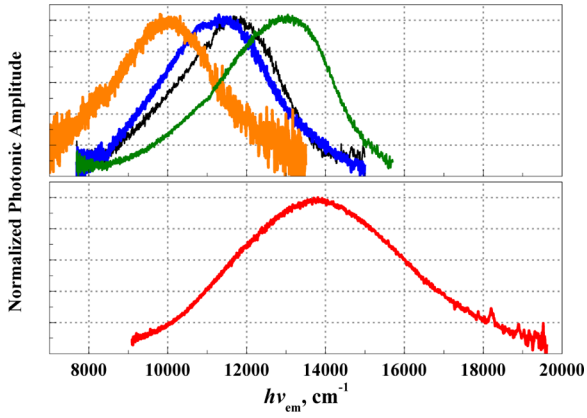

Figure 2. Emission spectra of the $[Ru(ND_3)_5(MDA)]^{2+}$ complexes at 77 K in butyronitrile. For the upper panel, MDA = ph-py, green; pz, black; 4,4′-bpy, blue; ac-py, orange. For the lower panel, MDA = d_5-py. Emission spectra were obtained by using a 0.2 mm slit width for spectra (without MDA = d_5-py) and a 0.5 mm slit width for spectrum of $[Ru(ND_3)_5(d_5\text{-py})]^{2+}$ ion.

contrasts with the MLCT excited state emission spectra of numerous ruthenium−PDA type complexes, PDA = polydentate aromatic ligand (bpy, tpy, etc.), many of which have well-characterized vibronic side bands.[4,6,11,63−65] Our observations are summarized in Table 1.

The emission bandwidths (fwhh) of $[Ru(ND_3)_5(MDA)]^{2+}$ in the upper panel of Figure 2, where MDA = pz, 4,4′-bpy, ac-py, and ph-py, are in the 3000−3500 cm^{-1} range, but the emission bandwidth of $[Ru(ND_3)_5(d_5\text{-py})]^{2+}$ is broader, 5000 cm^{-1}, in part because we had to use a wider spectrometer slit width (0.5 mm compared to 0.2 mm) to determine its spectrum, but the broad emission spectrum of this complex is also consistent with the very shallow ^{3}MLCT potential energy (PE) minimum found in the DFT modeling (described below). The difference between the 300 K absorption and 77 K emission maxima of pentaammine− and tetraammine−Ru complexes (9.9 ± 0.5 and 7.6 ± 0.8 $cm^{-1}/10^3$, respectively) is significantly larger than those found for the Ru−bpy chromophores (about 5−6 $cm^{-1}/10^3$)[36] and about 30% larger for the pentaammines than for the other Ru−MDA complexes.

The maxima of the 77 K emission spectra found for the $[Ru(NH_3)_5(MDA)]^{2+}$ complexes correlate with the MLCT

DOI: 10.1021/acs.inorgchem.5b01193
Inorg. Chem. 2015, 54, 8495−8508

Table 1. Summary of Ambient Absorption, 77 K Emission Spectra, and Emission Decay Constants of the Complexes[a]

code	complexes	$h\nu_{max}$(abs)[b]	77 K emission properties	
			$h\nu_{max}$(em)[b]	k_{obs}, μs^{-1}[c]
1	$[Ru(ND_3)_5(d_5\text{-py})]^{2+}$[d]	24.42	13.82	
2	$[Ru(NH_3)_5(ph\text{-py})]^{2+}$[d]	22.32	13.02	1.8
3	$[Ru(NH_3)_5(pz)]^{2+}$[d]	21.81	11.72	15
4	$[Ru(NH_3)_5(ac\text{-py})]^{2+}$[d]	19.80	10.02	29
5	$[Ru(NH_3)_5(4,4'\text{-bpy})]^{2+}$[d]	21.05	11.46	8.3
2-c	*cis*-$[Ru(NH_3)_4(ph\text{-py})_2]^{2+}$[e]	22.15	14.8	0.37
2-t	*trans*-$[Ru(NH_3)_4(ph\text{-py})_2]^{2+}$[e]	21.38	14.63	0.29
3-c	*cis*-$[Ru(NH_3)_4(pz)_2]^{2+}$[e]	21.98	13.50	3.6
3-t	*trans*-$[Ru(NH_3)_4(pz)_2]^{2+}$[e]	21.34	14.22	1.5
4-c	*cis*-$[Ru(NH_3)_4(ac\text{-py})_2]^{2+}$[e]	19.86	12.62	6.7
4-t	*trans*-$[Ru(NH_3)_4(ac\text{-py})_2]^{2+}$[e]	19.32	11.94	9.1
3′	*trans*-$[Ru(NH_3)_4(py)\ (pz)]^{2+}$[e]	21.76	12.92	2.9
3″	*mer*-$[Ru(NH_3)_3(bpyam)\ (pz)]^{2+}$[d]	21.80	13.67	1.9

[a]Dominant 300 K low-energy absorption maxima, $h\nu_{max}$(abs), determined in acetonitrile; emission maxima, $h\nu_{max}$(em), mean excited state decay rate constant, k_{obs}, determined at 77 K in butyronitrile glasses. [b]Energies in $cm^{-1}/10^3$. [c]Mean excited state decay rate constant, $k_{obs} = 1/\tau_{obs}$. [d]This work. [e]Ref 19.

absorption spectra, Figure 3. That the emission maxima vary in the same manner as the absorption maxima supports our

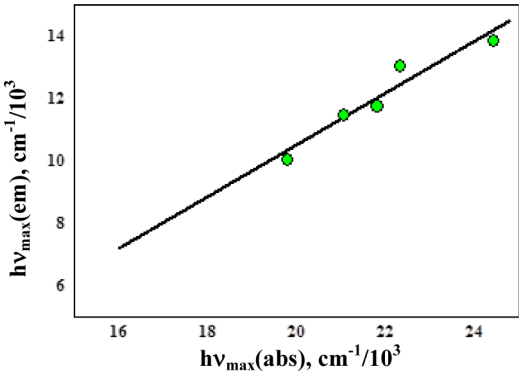

Figure 3. Correlations of the emission and MLCT absorption maxima for Ru–MDA chromophores **1**–**5** from Table 1.

assignment that these are emissions from ^{3}MLCT excited states; for a similar plot including the $[Ru(NH_3)_4(MDA)(MDA')]^{2+}$ complexes, see Supporting Information, Figure S1. The slope of the correlation in Figure 3 is about 0.8 ± 0.2 rather than 1.0, but this is probably a consequence of the scatter of data, the relatively limited energy range of the observations, and the DFT-based inference that the orbital occupations of the Franck–Condon excited states reached by absorption do not always correlate with those of the lowest energy ^{3}MLCT excited state.[19,36]

The $[Ru(NH_3)_5(MDA)]^{2+}$ complexes emit at lower energies, but Figures 3 and 4 indicate that their emission properties are consistent with those of the $[Ru(NH_3)_4(MDA)(MDA')]^{2+}$ chromophores. For any given energy, the ^{3}MLCT excited state lifetimes of all of the Ru–MDA chromophores are actually 3 to 6 times *longer* than those of the complexes with Ru–bpy chromophores with the same excited state energies; see also details in Supporting Information, Table S2.[41] This observation is important since it means that the weak emissions of this class of complexes are not the result of efficient ^{3}MLCT → ^{3}MC internal conversion at 77 K, such as that found for the $[Ru([14]aneS_4)\ (bpy)]^{2+}$ complex ([14]aneS$_4$ = 1,4,8,11-tetrathiacyclotetradecane).[20] We have now examined the

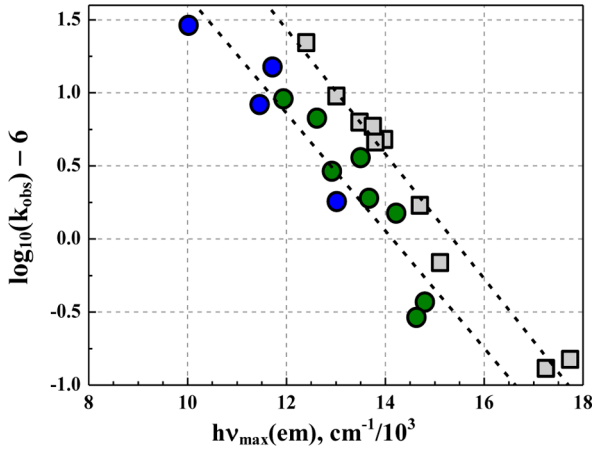

Figure 4. Correlation of the 77 K emission decay rate constants and the emission maxima for (Am = NH_3; en/2): $[Ru(bpy)_2(Am)_2]^{2+}$,[44] $[Ru(bpy)(NH_3)_3(MDA)]^{2+}$,[19] and $[Ru(bpy)(Am)_4]^{2+}$[44] (gray squares); *cis*-/*trans*-$[Ru(NH_3)_4(MDA)_2]^{2+}$, *trans*-$[Ru(NH_3)_4(py)(pz)]^{2+}$, and *mer*-$[Ru(NH_3)_3(bpyam)(pz)]^{2+}$ (green circles);[19] and $[Ru(NH_3)_5(MDA)]^{2+}$ (blue circles). The least-squares lines have a slope of (−0.43 ± 0.04) × 10^3 cm^{-1} and an intercept of 6.6 ± 0.6 for the Ru–bpy chromophores and a slope of (−0.40 ± 0.05) × 10^3 cm^{-1} and an intercept of 5.7 ± 0.6 for the Ru–MDA chromophores.

relaxation properties in Ru–MDA complexes that span an energy range of about 0.5 eV. The emission yields of the Ru–MDA chromophores tend to be much smaller than those of the simple monobpy complexes over this energy range,[19] and a more extensive report and discussion of the implications of this will be presented elsewhere.[66]

Computational Results. Figure 5 shows the ground S_0 and lowest energy triplet excited states ^{3}MLCT and $^3MC_{X(Y)}$ ($X(Y)$ designates that the distortion is along the Cartesian X axis and that there is a correlated distortion along the Y axis) for $[Ru(NH_3)_5(py)]^{2+}$; the calculated distortions in all Ru–L bonds in these excited states are compared in Table 2. The $^3MC_{X(Y)}$ excited state is calculated to be lower in energy than the lowest energy ^{3}MLCT state by about 880 cm^{-1} and is significantly distorted along one NH_3–Ru–NH_3 axis, with Ru–N_2 and Ru–N_5 bond distances of 2.614 and 2.615 Å,

DOI: 10.1021/acs.inorgchem.5b01193
Inorg. Chem. 2015, 54, 8495–8508

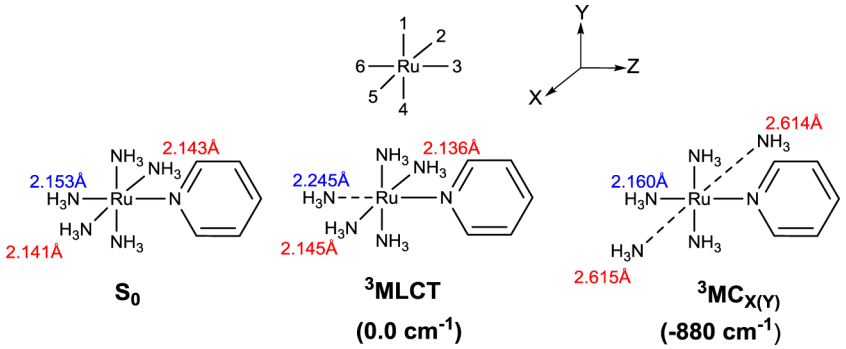

Figure 5. Comparison of the DFT-calculated structures of S_0, ^{3}MLCT, and $^3MC_{X(Y)}$ states and calculated relative energies of the ^{3}MLCT (arbitrarily set to zero) and $^3MC_{X(Y)}$ states of $[Ru(NH_3)_5(py)]^{2+}$. See Table 2 for calculated distortions of the other bonds.

Table 2. Calculated Bond Lengths of the Lowest Energy Electronic States of $[Ru(NH_3)_5(py)]^{2+}$

electonic state	Ru−L_1	Ru−L_2	Ru−L_3	Ru−L_4	Ru−L_5	Ru−L_6
S_0	2.142	2.143	2.064	2.142	2.141	2.153
^{3}MLCT	2.136	2.136	2.094	2.144	2.145	2.245
$^3MC_{X(Y)}$	2.158	2.614	2.102	2.171	2.615	2.160

respectively, compared to 2.143 and 2.141 Å, respectively, in the ground state S_0.

The spin density plots and the singly occupied molecular orbitals (SOMOs) of the ^{3}MLCT and $^3MC_{X(Y)}$ states of $[Ru(NH_3)_5(py)]^{2+}$ are shown in Figure 6. The Mulliken spin

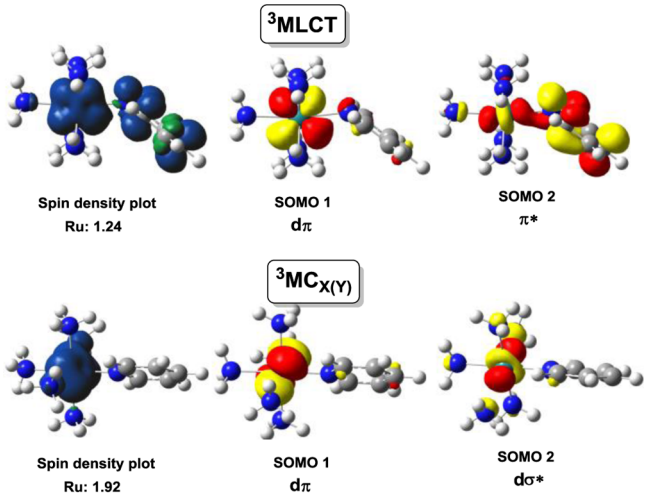

Figure 6. Spin density plots (isosurface value of 0.004 au) and singly occupied molecular orbitals (SOMOs) of ^{3}MLCT and $^3MC_{X(Y)}$ states of $[Ru(NH_3)_5(py)]^{2+}$. SOMOs are plotted with an isosurface value of 0.05 au.

density value, 1.24, found for the Ru center in ^{3}MLCT structure is unusually high; see Table 3. Analysis of the SOMOs shows that SOMO 1 is almost exclusively a dπ orbital on Ru, whereas the π^* SOMO 2 on the pyridine moiety has a significant contribution from one Ru dσ^* orbital (Figure 6). This contribution results in two noticeable distortions found in the ^{3}MLCT state: (a) to facilitate the overlap between the π^* orbital with the Ru dσ^* orbital, the pyridine moiety deviates significantly from the σ-plane in a solvent (SMD model; as noted previously)[19] and (b) bonding to the amine *trans* to the pyridine moiety is weakened, as can be seen from the Ru−NH_3

Table 3. Spin Densities for the ^{3}MLCT Excited States Calculated in This Work Compared to Some Literature Values

complex	calcd ^{3}MLCT excited state spin densities of Ru[a]
$[Ru(NH_3)_5(py)]^{2+}$	1.24
$[Ru(NH_3)_5(ph\text{-}py)]^{2+}$	0.92
$[Ru(NH_3)_5(pz)]^{2+}$	1.10
$[Ru(NH_3)_5(ac\text{-}py)]^{2+}$	0.98
$[Ru(NH_3)_5(4,4'\text{-}bpy)]^{2+}$	0.96
cis-$[Ru(NH_3)_4(ph\text{-}py)_2]^{2+}$	0.97
trans-$[Ru(NH_3)_4(ph\text{-}py)_2]^{2+}$	0.89
cis-$[Ru(NH_3)_4(pz)_2]^{2+}$	1.11
trans-$[Ru(NH_3)_4(pz)_2]^{2+}$	1.11
cis-$[Ru(NH_3)_4(ac\text{-}py)_2]^{2+}$	1.00
trans-$[Ru(NH_3)_4(ac\text{-}py)_2]^{2+}$	0.95
trans-$[Ru(NH_3)_4(py)(pz)]^{2+}$	1.09
$[Ru(NH_3)_4bpy]^{2+}$[b]	1.02
$[Ru(bpy)_3]^{2+}$[c]	0.90
$[Ru(NCCH_3)_4bpy]^{2+}$[d]	0.73
$[Ru([14]aneN_4)bpy]^{2+}$[b]	1.04
$[Ru([14]aneS_4)bpy]^{2+}$[d]	0.86
$[Ru([9]aneS_3)(CN)bpy]^{+}$[b]	0.82
$[Ru(NH_3)_2(bpy)_2]^{2+}$[b]	1.00
$[Ru(en)\ (bpy)_2]^{2+}$[b]	0.99
$[Ru(O_4C_2)_2(bpy)]$[b]	0.93

[a]This work except as indicated. [b]Ref 21. [c]Ref 67. [d]Ref 20.

bond distance of 2.245 Å in the ^{3}MLCT state compared to 2.153 Å in the ground S_0 state (Figure 5). This mixing of the pyridine π^* and Ru dσ^* orbitals can be described as configurational mixing between a pure ^{3}MLCT state and a pure ^3MC_Z state that is distorted along the NH_3−Ru−N(py) axis. These two states are apparently close in energy, which would favor mixing; however, this significant ^{3}MLCT/^{3}MC mixing contrasts markedly to the very weak mixing found in our modeling of the $[Ru([14]aneS_4)(bpy)]^{2+}$ complex[20] (noted above). In the present case, the $^3MC_{X(Y)}$ state is distorted along the NH_3−Ru−NH_3 axis and is found to have a spin density value of 1.92 on the Ru center, and the two SOMOs are found to be almost exclusively Ru-based dπ and dσ^* orbitals (Figure 6).

Figure 7 illustrates that two NH_3−Ru−NH_3 axes (X and Y axes) are nearly equivalent in the ^{3}MC state of the $[Ru(NH_3)_5(py)]^{2+}$ complex. The lowest energy ^{3}MC excited state of this complex has two PE minima, $^3MC_{X(Y)}$ and $^3MC_{(X)Y}$, corresponding to similar distortions along the NH_3−Ru−

DOI: 10.1021/acs.inorgchem.5b01193
Inorg. Chem. 2015, 54, 8495−8508

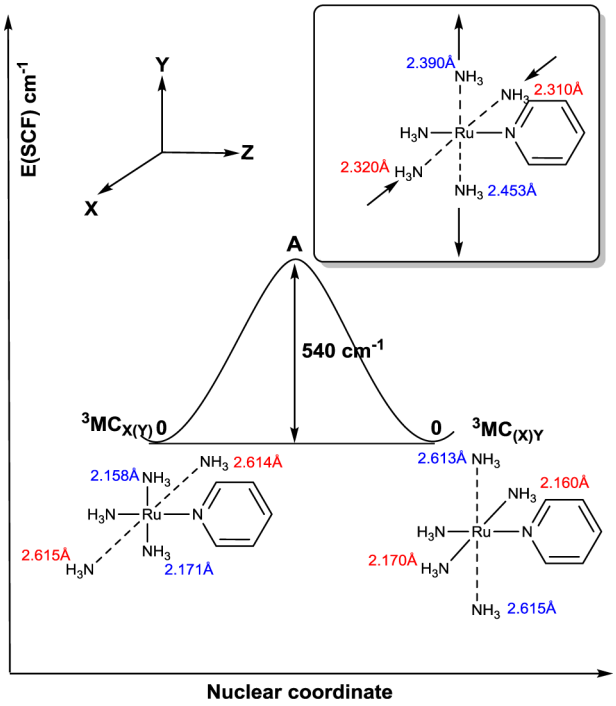

Figure 7. Energy relations for the pseudo-Jahn–Teller-like distorted $^3MC_{(X,Y)}$ states of $[Ru(NH_3)_5(py)]^{2+}$. The calculated $^3MC_{X(Y)}$ and $^3MC_{(X)Y}$ structures show distortion along different NH_3–Ru–NH_3 axes. The barrier for their interconversion is calculated to be small, about 540 cm^{-1}. The nuclear coordinate displayed here corresponds to an antisymmetric stretch (associated with an imaginary frequency of about 98 cm^{-1}) about **A** in the equatorial $Ru(NH_3)_4$ plane.

NH_3 axes of the equatorial $Ru(NH_3)_4$ plane. They can be readily interconverted through transition state, **A**, which is located at 540 cm^{-1} higher in energy. Transformation from $^3MC_{X(Y)}$ to $^3MC_{(X)Y}$ or *vice versa* requires one NH_3–Ru–NH_3 axis to be compressed while the other NH_3–Ru–NH_3 axis is elongated, consistent with a pseudo-Jahn–Teller-like distortion.[68,69] The resulting coordination sphere motions correspond to an antisymmetric stretch leading to **A**, and this vibration is associated with an imaginary frequency of about 98 cm^{-1}. Since the complex symmetry is lower than C_{4v}, the *X* and *Y* axes are not degenerate and the distortions at point **A** are not identical. This pattern of $^3MC_{X(Y)}$ excited state distortions is typical of the $[Ru(NH_3)_5(MDA)]^{2+}$ complexes, all of which have approximately C_{4v} microsymmetry around Ru.

At the maximum of the PE curve (**A**) in Figure 7 the SOMOs correspond to unpaired electrons in the d_{xy} and $d_{x^2-y^2}$ orbitals, as shown in Figure 8. The bond lengths of the lowest energy bound states of $[Ru(NH_3)_5(py)]^{2+}$ are summarized for comparison purposes in Table 4.

The ^{3}MLCT state of $[Ru(NH_3)_5(py)]^{2+}$ complex has a significant contribution from a ^3MC_Z state that is distorted along the NH_3–Ru–N(py) axis. As a result, the metal–ligand interactions in that axis are weakened in the ^{3}MLCT state in which the pyridine ligand is found to be prone to dissociation. As illustrated in Figure 9, elongation of the Ru–NH_3 and Ru–N(py) bond lengths from the ^{3}MLCT structure leads to the formation of a ^3MC_Z state, and this state is dissociative; the scan of the dissociative coordinate was terminated for a Ru–py bond length of 2.44 Å. This process with a very small energy barrier is predicted to be very feasible even at low temperature, where the emission spectrum of the perdeuterated complex was

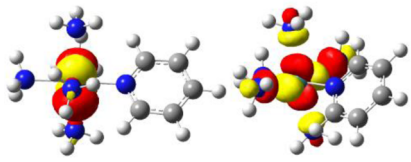

SOMO1 (d_{xy}) of point A SOMO2 (d_{x2-y2}) of point A

Figure 8. Singly occupied molecular orbitals (SOMOs) at transition state **A** between PE minima of the $^3MC_{(X,Y)}$ state of $[Ru(NH_3)_5(py)]^{2+}$. SOMOs are plotted with an isosurface value of 0.05 au.

recorded. On the basis of these observations, it is likely that the observation that a weak emission was observed only for the perdeuterated complex is due to its smaller zeropoint energy and consequently somewhat larger PE barrier for dissociation. The resulting ^3MC_Z state is dissociative, and it initially forms a five-coordinate $[Ru(NH_3)_5]^{2+}$ complex and free py is trapped in a solvent cage.

The calculated ^{3}MC excited state properties of the $[Ru(NH_3)_5(ph\text{-}py)]^{2+}$ complex contrast markedly to those of $[Ru(NH_3)_5(py)]^{2+}$. Unlike the pyridine complex, the calculated structures in Figure 10, the relative energies, spin density plots, and SOMOs of the ^{3}MLCT and $^3MC_{X(Y)}$ states of $[Ru(NH_3)_5(ph\text{-}py)]^{2+}$ indicate that the ^{3}MLCT excited state of the phenylpyridine complex does not have any significant contribution from a ^3MC_Z state so that it can be considered to be a pure ^{3}MLCT state at its PE minimum. The calculated spin density on Ru is 0.92, and SOMO 2 is a π^* orbital predominantly on the phenylpyridine ligand. Since the ^{3}MLCT state does not have any significant contribution from a distorted ^3MC_Z state, the structural distortions found in the ^{3}MLCT state of $[Ru(NH_3)_5(py)]^{2+}$ are absent at the PE minimum in the case of the $[Ru(NH_3)_5(ph\text{-}py)]^{2+}$ complex. The phenylpyridine moiety does not show any significant deviation from the σ-plane at the PE minimum, unlike py in $[Ru(NH_3)_5(py)]^{2+}$, and the bonding to the amine *trans* to the phenylpyridine moiety is not significantly weakened, as can be seen from the Ru–NH_3 bond distance of 2.160 Å in the ^{3}MLCT state compared to 2.153 Å in the ground state. However, there is mixing at the IC transition state (**A** in Figure 7), and the ph-py ligand is folded at this point. Phenylpyridine is a better electron acceptor than the pyridine moiety, and the ^{3}MLCT state is calculated to be about 770 cm^{-1} lower in energy than the $^3MC_{X(Y)}$ state in the case of $[Ru(NH_3)_5(ph\text{-}py)]^{2+}$, whereas the reverse is the case for the $[Ru(NH_3)_5(py)]^{2+}$ complex.

The absence of structural distortions in the ^{3}MLCT state of $[Ru(NH_3)_5(ph\text{-}py)]^{2+}$ complex results in a stronger metal–chromophore ligand bonding interaction than that found in the case of the $[Ru(NH_3)_5(py)]^{2+}$ complex. The Ru–N(ph-py) bond distance in the ^{3}MLCT state becomes shorter: 2.027 Å compared to 2.061 Å in S_0; in contrast, the Ru–N(py) bond length is found to be longer in the ^{3}MLCT than in the S_0 state of the $[Ru(NH_3)_5(py)]^{2+}$ complex (Table 2). The energy profile for the dissociation of the phenylpyridine moiety from the ^{3}MLCT state passes through a maximum point that is about 1200 cm^{-1} higher in energy than the PE minimum of the ^{3}MLCT state (Figure 11). The ^3MC_Z state obtained is unstable with respect to the dissociation of the phenylpyridine molecule and formation of a five-coordinate $[Ru(NH_3)_5]^{2+}$ complex (initially in a solvent cage). This result is in contrast to the case for the $[Ru(NH_3)_5(py)]^{2+}$ complex, where there is very little

DOI: 10.1021/acs.inorgchem.5b01193
Inorg. Chem. 2015, 54, 8495–8508

Table 4. Calculated Bond Lengths for the Lowest Energy Electronic States of $[Ru(NH_3)_5py]^{2+}$

		calcd avg Ru−N bond lengths, Å			
state	distortion axis	$Ru-(NH_3)_X$	$Ru-(NH_3)_Y$	$Ru-(NH_3)_Z$	Ru−py
S_0	2.14	2.14	2.15	2.06	
^{3}MLCT	2.14	2.14	2.25	2.09	
$^3MC_{(X,Y)}$	*X* axis	2.61	2.16	2.16	2.10
	Y axis	2.17	2.61	2.16	2.10
	A	2.32	2.42	2.15	2.08

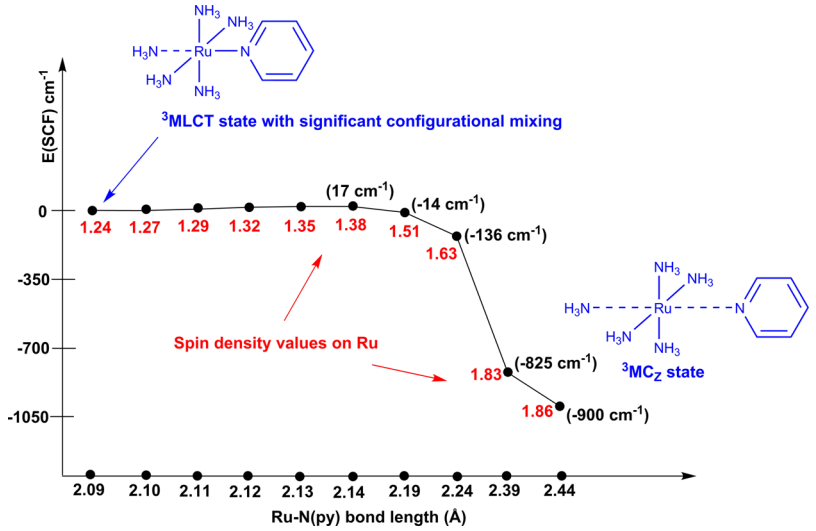

Figure 9. Calculated energy profile for transformation of the ^{3}MLCT state of $[Ru(NH_3)_5(py)]^{2+}$ into a ^3MC_Z state. Ru−N(py) and Ru−NH_3 bond distances are elongated by 0.01 Å at each point starting from the ^{3}MLCT state until the maximum point (17 cm^{-1}) of the energy profile was reached. Note that the bond lengths on the abscissa are the Ru−N(py) bond lengths assumed in the calculation of energies excited state along the *Z* coordinate and the scale is not linear: the increment of the bond distances has been increased by 0.05 Å for each point after that maximum point of the energy profile. The rest of the molecular geometry was reoptimized in each case. Note that a unique energy cannot be defined for the dissociative ^3MC_Z state.

barrier for the ^{3}MLCT state to dissociate the pyridine moiety. However, for both complexes, the ^{3}MLCT/^3MC_Z crossing is smooth (adiabatic), and this implies significant ^{3}MLCT/^3MC_Z configurational mixing at the transition state for the crossing.

We have calculated the energy differences between the lowest energy bound ^{3}MLCT and $^3MC_{X(Y)}$ states for several $[Ru(NH_3)_5(MDA)]^{2+}$ and $[Ru(NH_3)_4(MDA)_2]^{2+}$ complexes, and we used these calculated differences to estimate the energies of the lowest energy ^{3}MC excited states for these complexes in Table 3 by referencing them to observed emission maxima of the complexes for $E(^3MLCT)$ from Table 1. This referencing of $E(^3MC)$ to the emission maxima for $^3MLCT \rightarrow S_0$ necessarily contains a reorganizational energy contribution that arises from the coordination sphere distortions in low-frequency vibrational modes of ^{3}MLCT. Since the emission spectra found for the $[Ru(NH_3)_5(MDA)]^{2+}$ complexes are broad with no resolved vibronic components, this is an underestimate of the $E^{0'0}(^3MC)$ energies. The emission spectrum of the $[Ru(NH_3)_4bpy]^{2+}$ complex has some resolved vibronic features, and its DFT modeling suggests that $E^{0'0}(^3MLCT)$ is about 200 cm^{-1} higher in energy than $h\nu_{max}$(em) for component bandwidths of about 400 cm^{-1}.[18] When the observed spectra are broad and have no resolved vibronic components, the difference between $h\nu_{max}$(em) and $E^{0'0}(^3MLCT)$ is expected to be substantially larger,[44] and we would expect the actual $E^{0'0}(^3MC)$ energies of the $[Ru(NH_3)_5(MDA)]^{2+}$ complexes to be closer to those of the $[Ru(NH_3)_4(MDA)_2]^{2+}$ complexes than is suggested by entries in Table 5.

DISCUSSION

This is the first report of emission in $[Ru(NH_3)_5(MDA)]^{2+}$ complexes. The resulting emission spectra combined with those of the $[Ru(NH_3)_4(MDA)_2]^{2+}$ complexes and computational modeling of the lowest energy triplet excited states provide some new insights into the photochemistry of these complexes and the patterns of variations in ^{3}MC excited state energies. Several of the pentaammine complexes emit weakly in 77 K glasses, with the weakest being the $[Ru(ND_3)_5(d_5\text{-}py)]^{2+}$ complex, for which perdeuteration and wide spectrometer slits were necessary in order for us to detect the emission. For most of these complexes, the DFT calculations indicate that the lowest energy excited state is a ^{3}MLCT state. This, and correlations of the emission energies with absorption band energies (Figures 3 and Supporting Information S2)[41] and with the emission decay lifetimes (Figure 4), supports the assignment of a ^{3}MLCT origin for these emissions. We have previously reported DFT calculations that show that the low-energy ^{3}MLCT and $^3MC_{X(Y)}$ states have similar energies for *trans*-$[Ru(NH_3)_4(pz)_2]^{2+}$ and *trans*-$[Ru(NH_3)_4(py)(pz)]^{2+}$[19] but that their ^{3}MLCT emissions are very weak due to very small quantum yields, and this appears to be generally the case for the $[Ru(NH_3)_5(MDA)]^{2+}$ and $[Ru(NH_3)_4(MDA)_2]^{2+}$ complexes.[70]

DOI: 10.1021/acs.inorgchem.5b01193
Inorg. Chem. 2015, 54, 8495−8508

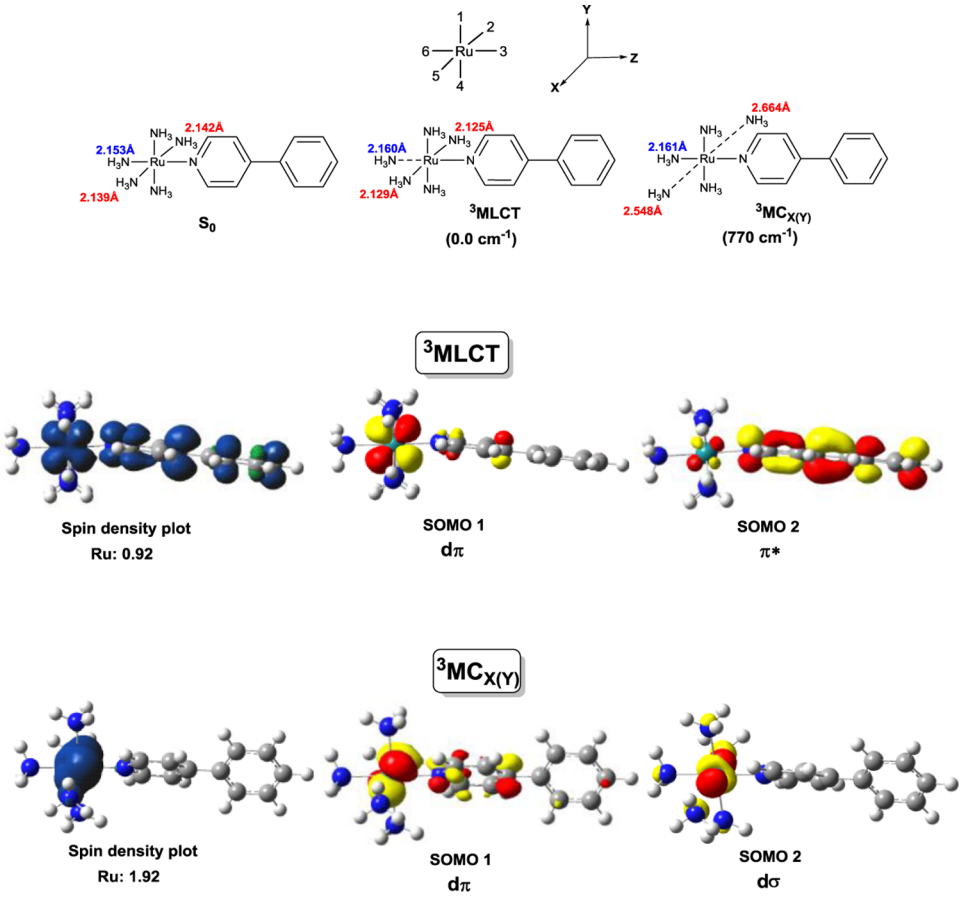

Figure 10. Structures, relative energies, spin density plots (isosurface value of 0.004 au), and singly occupied molecular orbitals (SOMOs) of ^{3}MLCT and $^3MC_{X(Y)}$ states of $[Ru(NH_3)_5(ph\text{-}py)]^{2+}$. SOMOs are plotted with an isosurface value of 0.05 au. The energy of the ^{3}MLCT state is arbitrarily set to zero. See Table 5 for estimated energies relative to S_0.

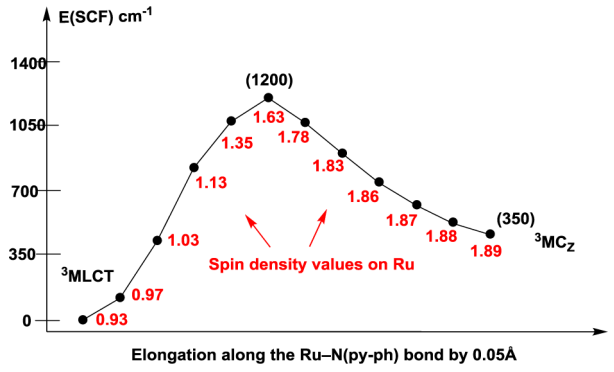

Figure 11. Transformation of the ^{3}MLCT state of $[Ru(NH_3)_5(ph\text{-}py)]^{2+}$ into a ^3MC_Z state. The Ru–N(ph-py) bond distance is elongated by 0.05 Å at each point starting from the ^{3}MLCT state, and the rest of the molecular geometry is reoptimized in each case. The ^3MC_Z electronic configuration obtained from the scan is dissociative. Other details are as those in the caption of Figure 9.

Since the difficulty in detecting emissions from this class of complexes is often attributed to efficient internal conversion to a similar, or lower, energy ^{3}MC excited state,[14] we have used DFT approaches to estimate their energies, to evaluate internal conversion barriers, and to construct more detailed models of the ^{3}MC excited states for some of them. The experimental spectroscopic observations and the computational modeling of the lowest energy triplet excited states in these complexes have implications for the photochemical reaction mechanisms of this class of complexes, and they point to some important considerations in the design of transition metal complex photosensitizers.

General Observations on the Role of ^{3}MC Excited States in the Quenching of Ru–MDA ^{3}MLCT Excited States. Furthermore, the estimated energies of the lowest energy ^{3}MC excited states in Table 5 suggest that there is little variation in $E(^3MC)$, whereas the energies of the ^{3}MLCT excited states vary a great deal, and in most cases, the latter are the lowest energy excited states. Thus, the weaker emissions of the Ru–MDA systems at 77 K cannot generally be the result of more efficient internal conversion to a ^{3}MC excited state.

Computational Modeling of the ^{3}MC States and Its Implications. The DFT modeling of the triplet manifolds of the $[Ru(NH_3)_5(MDA)]^{2+}$ and *trans*-$[Ru(NH_3)_4(MDA)(MDA')]^{2+}$ complexes indicates relatively simple patterns of their excited state distortions and energies. In the octahedral limit, as for $[Ru(NH_3)_6]^{2+}$, the lowest energy triplet excited state, with a nominal $\{\pi(d)\sigma^*(d)\}$ electronic configuration, would be tetragonally distorted into two states: one predominately distorted in the *X*, *Y* plane ($^3MC_{(X,Y)}$) and the other along the *Z* axis (^3MC_Z).[68,71−73] Since the pentaammines and *trans*-tetraammines have approximately C_{4v} symmetry, similar Jahn–Teller distortions are expected; the triplet excited states of the lower symmetry *cis*-tetraammines and *mer*-triammines have no orbital degeneracies. However, the computational modeling indicates that the $^3MC_{(X,Y)}$ state is the lowest energy Jahn–

DOI: 10.1021/acs.inorgchem.5b01193
Inorg. Chem. 2015, 54, 8495−8508

Table 5. Estimated Energies of the Lowest Energy ^{3}MC Excited States for Some Ru^{II} Complexes[a]

complexes	obsvd $h\nu_{max}$(em)[b]	calcd $\Delta E(^3\text{MLCT}/^3\text{MC}_{X(Y)})$ ($\Delta E(^3\text{MLCT}/^3\text{MC}_Z)$)[c]	relative $E(^3\text{MC}_{X(Y)})$ ($E(^3\text{MC}_Z)$)[d]
$[Ru(NH_3)_5(py)]^{2+}$	13.8	−0.94	12.8
$[Ru(NH_3)_5(ph\text{-}py)]^{2+}$	13.02	0.77	13.8
$[Ru(NH_3)_5(pz)]^{2+}$	11.72	1.89	13.6
$[Ru(NH_3)_5(ac\text{-}py)]^{2+}$	10.02	3.67	13.7
$[Ru(NH_3)_5(4,4'\text{-}bpy)]^{2+}$	11.46	2.31	13.8
cis-$[Ru(NH_3)_4(ph\text{-}py)_2]^{2+}$	14.8	0.14	14.9
trans-$[Ru(NH_3)_4(ph\text{-}py)_2]^{2+}$	14.63	0.14 (−0.46)[e]	14.8 (14.2)
cis-$[Ru(NH_3)_4(pz)_2]^{2+}$	13.50	1.05	14.6
trans-$[Ru(NH_3)_4(pz)_2]^{2+}$	14.22	0.46 (−0.35)[e]	14.7 (13.9)
cis-$[Ru(NH_3)_4(ac\text{-}py)_2]^{2+}$	12.62	2.84	15.5 (13.9)
trans-$[Ru(NH_3)_4(ac\text{-}py)_2]^{2+}$	11.94	2.48 (1.92)[e]	14.4
trans-$[Ru(NH_3)_4(py)(pz)]^{2+}$	12.92	1.19	14.1
$[Ru(NH_3)_4bpy]^{2+}$	12.4	2.9	15.3
$[Ru(bpy)_3]^{2+}$	17.2	2.9[f]	20.1
$[Ru(NCCH_3)_4bpy]^{2+}$	19.4[g]	−3.8	15.6
$[Ru([14]aneN_4)bpy]^{2+}$[i]	13.1[h]	−0.1[i]	13.0
$[Ru([14]aneS_4)bpy]^{2+}$	19.7[g]	−3.6[g]	16.1
$[Ru([9]aneS_3)(CN)bpy]^{+}$[i]	19.2	−1.4	17.8
$[Ru(NH_3)_2(bpy)_2]^{2+}$[i]	14.7	2.0	16.7
$[Ru(en)_2(bpy)]^{2+}$[i]	15.1	2.1	17.2
$[Ru(O_4C_2)(bpy)_2]$[i]	14.2	4.1	18.3

[a]Energies in $cm^{-1}/10^3$. [b]77 K emission energy maxima from Table 1 except as indicated. [c]$E(^3\text{MC}) - E(^3\text{MLCT})$ (the difference in the energies of PE minima). [d]$h\nu_{max}$(em) + ΔE(MLCT/MC); using $h\nu_{max}$(em) instead of $E^{0'0}(^3\text{MLCT})$ underestimates $E^{0'0}(^3\text{MC})$ possibly by 300−1000 cm^{-1},[18,44] largely due to the bandwidth issues discussed in the text, and the uncertainty in the referencing is not the same for all complexes. [e]The $^3\text{MC}_Z$ state is weakly bound for these complexes. The current level of calculations agrees with the earlier report.[19] [f]Ref 15. [g]Ref 18. [h]Ref 20. [i]Ref 21.

Teller ^{3}MC excited state in $[Ru(NH_3)_5(MDA)]^{2+}$ complexes but that this state is pseudo-Jahn−Teller-distorted along the *X* and *Y* axes ($^3\text{MC}_{X(Y)}$ and $^3\text{MC}_{(X)Y}$, respectively), apparently as a result of mixing with a somewhat higher energy excited state.[69] The Jahn−Teller analyses of the absorption spectra of $[Co(NH_3)_6]^{3+}$[73] and of the emission spectra of $[Rh(NH_3)_6]^{3+}$,[71] both with nd^6 electronic configurations analogous to Ru^{II} complexes, indicate that their lowest energy ^{3}MC excited states involve population of $d_{x^2-y^2}$ orbitals and totally symmetric, breathing type of distortions of the four M−L bonds in the *X*, *Y* plane.

The structural distortions are much smaller in the ^{3}MLCT state of $[Ru(NH_3)_5(py\text{-}ph)]^{2+}$ than in the $[Ru(NH_3)_5(py)]^{2+}$ complex, and its calculated spin density is smaller because the lower energy ^{3}MLCT excited state of the former and the probaby similar $^3\text{MC}_Z$ excited state energies lead to less mixing (Figure 12). Furthermore, the $^3\text{MLCT} \rightarrow {}^3\text{MC}_Z$ internal conversion of $[Ru(NH_3)_5(ph\text{-}py)]^{2+}$ has a significant barrier (about 1200 cm^{-1}; compare Figures 9 and 11) and largely rules out this process as a significant ^{3}MLCT quenching mechanism for this complex at 77 K. The $^3\text{MC}_Z$ electronic configuration that results from this IC process is unstable with respect to the dissociation of the phenylpyridine molecule and formation of a five-coordinate $[Ru(NH_3)_5]^{2+}$ complex. This result is in contrast to the $[Ru(NH_3)_5(py)]^{2+}$ ^{3}MLCT excited state, for which the py ligand readily dissociates in a nearly barrierless pathway. Although the dissociative $^3\text{MC}_Z$ excited states do not have well-defined energies, we can make comparisons of calculated orbital energies as in Figure 12B.

Overall, our observations are consistent with the Jahn−Teller splitting of the metal-centered excited states of the $[Ru(NH_3)_5(MDA)]^{2+}$ complexes, with the higher state tending to be distorted along the *Z* axis ($^3\text{MC}_Z$) and the lower energy state ($^3\text{MC}_{(X,Y)}$), along the *X* and *Y* axes, as expected based on the excited states of nd^6 complexes with O_h symmetry.[68,71−73] However, in the lower symmetry complexes examined here, our DFT calculations indicate that Ru−L bonding along the *Z* axis is somewhat weaker (by about 1000 cm^{-1}) than that along the *X* and *Y* axes, contributing to relatively small energy differences between the $^3\text{MC}_{(X,Y)}$ and $^3\text{MC}_Z$ states, and that the $^3\text{MC}_{(X,Y)}$ state in these complexes is further split into two weakly bound states that are distorted along different $H_3N-Ru-NH_3$ axes. The energies of the $M_{X(Y)}$ (and $M_{(X)Y}$) states are 15 000 ± 1000 cm^{-1}, nearly independent of MDA and close to the calculated energy for breaking two $Ru-NH_3$ bonds of the ground state (about 19 000 cm^{-1}). The computational modeling indicates that, at least for the $[Ru(NH_3)_5(py)]^{2+}$ and $[Ru(NH_3)_5(ph\text{-}py)]^{2+}$ complexes, internal conversion from the lowest energy ^{3}MLCT excited state leads to population of the $^3\text{MC}_Z$ excited state and that this state is dissociative in most, but not all, of the complexes with Ru−MDA chromophores.

The Exceptional Excited State Properties of the $[Ru(NH_3)_5(py)]^{2+}$ Complex. As indicated in Figure 9, the lowest energy ^{3}MLCT excited state of this complex can cross smoothly, and with almost no PE barrier, to the $^3\text{MC}_Z$ excited state. This, combined with the large spin density calculated (1.24; see Figure 6 and Table 3) for the Ru center of the ^{3}MLCT state, indicates that there is considerable configurational mixing between these states. This contrasts with the abrupt IC transitions that we have found in the modeling of other complexes,[20,21] but more strikingly, it contrasts with our observations on the $[Ru([14]aneS_4)bpy]^{2+}$ complex, for which we also calculated a nearly barrierless $^3\text{MLCT} \rightarrow {}^3$MC IC transition that was abrupt and for which the relatively well-resolved vibronic components of the emission also supported the inferred weak mixing between these excited states. It seems likely that the apparent contrasts in $^3\text{MLCT}/^3$MC electronic mixing arise from the differences in the spatial orientations of

DOI: 10.1021/acs.inorgchem.5b01193
Inorg. Chem. 2015, 54, 8495−8508

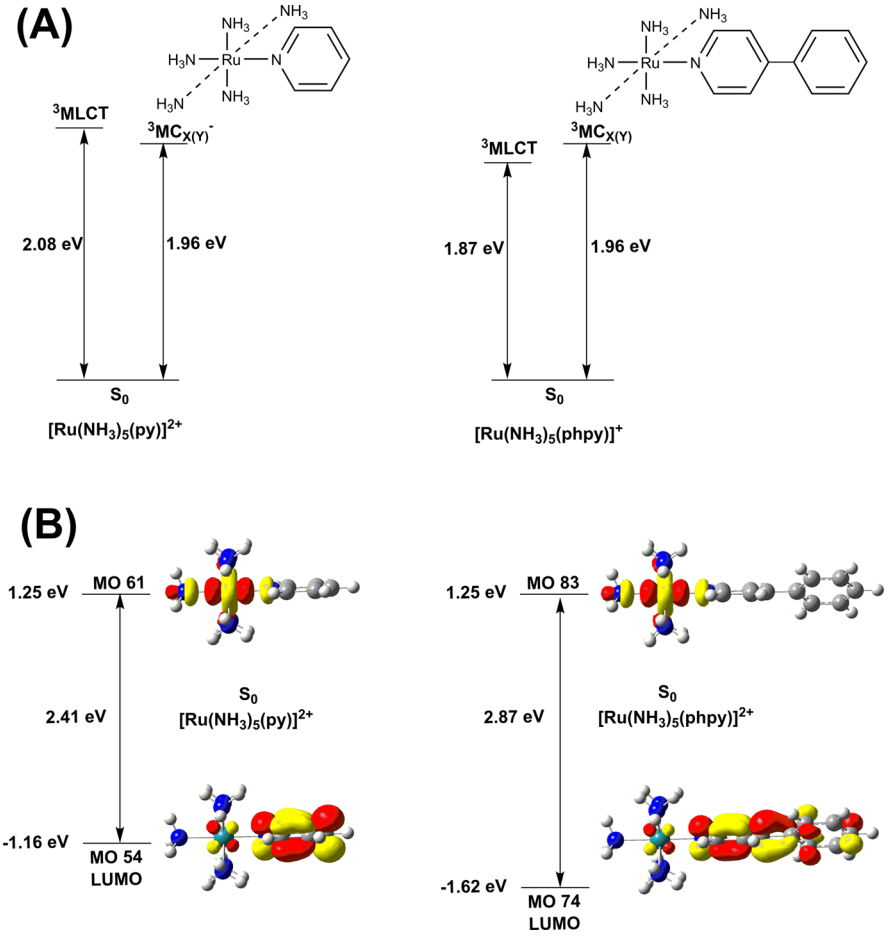

Figure 12. Comparison of the excited state energies for $[Ru(NH_3)_5(ph\text{-}py)]^{2+}$ and $[Ru(NH_3)_5(py)]^{2+}$. (A) The ^{3}MLCT state is lower in energy for $[Ru(NH_3)_5(ph\text{-}py)]^{2+}$ than it is for the $[Ru(NH_3)_5(py)]^{2+}$ complex, whereas the $^3MC_{X(Y)}$ states are essentially isoenergetic for both complexes. (B) The π^*(MDA) orbital (LUMO for S_0) is more stabilized in the case of the extended π-conjugated phenylpyridine system compared to that of the pyridine complex, whereas the Ru dσ^* orbitals (S_0 MOs 61 and 83) are isoenergetic for these complexes, and as a result, there is a larger energy difference between the π^*(MDA) and dσ^*(Ru) orbitals in the case of the $[Ru(NH_3)_5(ph\text{-}py)]^{2+}$ complex than that found in $[Ru(NH_3)_5(py)]^{2+}$. This leads to a stronger mixing between those two orbitals, as found in the SOMO 2 of the ^{3}MLCT state of the $[Ru(NH_3)_5(py)]^{2+}$ complex (Figure 6) compared to no mixing found in the SOMO 2 of the ^{3}MLCT state of $[Ru(NH_3)_5(ph\text{-}py)]^{2+}$ (Figure 10).

the aromatic acceptor ligands of these complexes: the bpy ligand of $[Ru([14]aneS_4)(bpy)]^{2+}$ is stereochemically constrained to lie very nearly in a Cartesian plane, whereas the py of $[Ru(NH_3)_5(py)]^{2+}$ is both rotated and folded in its ^{3}MLCT excited state, and this may result in better dπ/pπ spatial overlap between orbitals of Ru and py; however, this py/Ru mixing appears to be very weak since the folding of the py ligand does not occur in calculations performed without solvent.[19]

Durante and Ford[16] reported a relatively long-lived singlet transient intermediate, ^{1}**I**, formed in the flash photolysis of this complex, which they described in terms of Scheme 1.[16] This scheme involves a ^{3}MLCT → ^{3}MC* internal conversion, where MC* is proposed as the immediate excited state precursor of the transient ^{1}**I**. The intermediate ^{1}**I** can either undergo aquation to form $[Ru(NH_3)_5(H_2O)]^{2+}$ or regenerate the S_0 state.

The structure of ^{1}**I** was proposed to have one of the following two configurations: [16] (a) with a 90° rotation of the pyridine ring from the normal Ru−N bond axis to form a bond-localized cyclic triene system with a C═N(py) π-bond to the Ru center (**I**(**A**) in Figure 13) or (b) with the aromatic pyridine ring at an oblique angle to the normal Ru−N bond axis (**I**(**B**) in Figure 13). Our DFT calculations find that both of these

Scheme 1. Scheme Proposed by Durante and Ford[16] for the Formation of the Transient Intermediate, ^{1}I, in the Flash Photolysis Experiment of $[Ru(NH_3)_5(py)]^{2+}$[a]

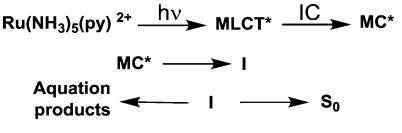

[a] **I** is formed from the metal-centered excited state MC* and decays either by transformation into the ground singlet state S_0 or by forming the $[Ru(NH_3)_5(H_2O)]^{2+}$ aquation product. Note that this scheme differs in some details from the results of the DFT modeling.

structures are unstable with regard to the conversion into the S_0 structure where the pyridine moiety is σ-bonded to Ru. A closely related alternative intermediate, **I**′, has been located by DFT modeling, where the pyridine ring is π-bonded to the Ru center using one C═C instead of the C═N double bond. The C═C π-bond is expected to be a better donor than the C═N π-bond to the Ru(II) center. The calculations indicate that the pyridine ring retains an oblique angle to the normal Ru−N bond axis as in the ^{3}MLCT excited state and that it resembles more a bond-localized cyclic triene system than an aromatic

DOI: 10.1021/acs.inorgchem.5b01193
Inorg. Chem. 2015, 54, 8495−8508

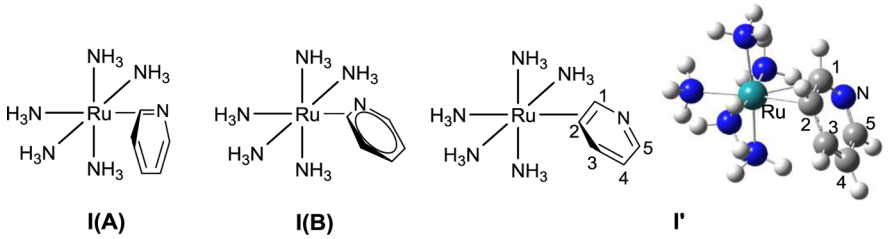

Figure 13. Comparison of the photochemical intermediate structures postulated by Durante and Ford (A and B)[16] to that found in DFT modeling. The DFT modeling found that the pyridine moiety binds to the Ru center in a η^2-fashion involving one C═C bond, as shown in the optimized geometry of **I′**. The other configurations, **I**(**A**) and **I**(**B**), are found to be unstable and readily transform into the S_0 structure, where the pyridine ring is σ-bonded to Ru.

ring. The calculated C_1-C_2, C_3-C_4, and C_5-N bond distances are 1.420, 1.373, and 1.313 Å, respectively, whereas the other C_2-C_3, C_4-C_5, and C_1-N bond distances are found to be longer, 1.428, 1.423, and 1.383 Å, respectively. Also, the hydrogen atoms on C_1 and C_2 deviate about 19° from the plane of the py-ring, illustrating the nonplanarity of the pyridine moiety and significant back bonding from the Ru(II) center into the π^* orbital of the coordinated C−C bond, consistent with the Dewar−Chatt−Duncanson model.[74−76]

The qualitative energy relationships of the singlet transient intermediate **I′** and the S_0 state that result from the calculations are illustrated in Figure 14, and a possible pathway for the formation and decay of the intermediate species is proposed. Since the ^3MC_Z state is dissociative, its energy is not readily compared to those of the bound states. The dissociation of py along the dissociative coordinate would initially result in the $Ru(NH_3)_5^{2+}$ fragment and py being in close proximity in a solvent cage. The DFT modeling indicates that the most stable $Ru(NH_3)_5^{2+}$ species is square a pyramidyl singlet, and the solvent cage species can either diffuse apart or recombine with recombination resulting in either the S_0 state or **I′**. The recombination reactions involve some rotation of py.

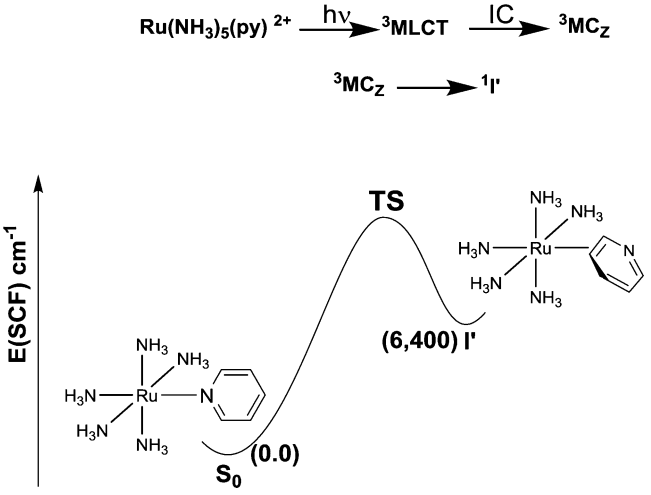

Figure 14. Formation of the intermediate ^{1}**I′** and a qualitative representation of its decay into the ground state. The reactions at the top of the figure identify MC* and ^{1}**I** of Scheme 1. The DFT calculations indicate that ^{1}**I′** is calculated to be about 6400 cm^{-1} higher in energy than the S_0 state. Our calculations also indicate that the $Ru(NH_3)_5^{2+}$ fragment has singlet spin multiplicity and that the energy of the dissociation limit of the ^3MC_Z state corresponding to this fragment plus py is about 8000 cm^{-1} relative to S_0. This is an upper limit for TS, so the barrier to regenerating S_0 from ^{1}**I′** is calculated to be less than or equal to 1600 cm^{-1}.

The Relative Energies of ^{3}MC Excited States and Their Role in Quenching the Lowest Energy Excited States. There is a rough correlation of the k_{obs} values from Table 1 with the values of ΔE(MLCT/MC) in Table 5 (Supporting Information Figure S3),[41] with k_{obs} tending to increase as ΔE(MLCT/MC) increases. This is not a causal relationship; rather, it is the result of the nearly constant values of $E(^3MC_{X(Y)})$ while $E(^3MLCT)$ varies by about 4000 cm^{-1}. This is consistent with the Ru−MDA emission decay rates being determined largely by the nonradiative relaxation of the ^{3}MLCT excited states to populate ground state vibrational modes (k_{NRD}):[1,3] $k_{obs} \approx k_{NRD} \gg (k_{IC} + k_{RAD})$, where k_{IC} and k_{RAD} are the $^3MLCT \rightarrow {}^3MC$ internal conversion and the radiative rate constants, respectively.

When referenced to the energy of the observed emission maxima, the lowest energy calculated ^{3}MC excited state energies vary over a relatively narrow range (Figure 15). As illustrated in Figure 15A, the estimated ^{3}MC excited state energies, based on $h\nu_{max}(em) + \Delta E(^3MLCT/^3MC)_{calcd}$, for the $[Ru(NH_3)_5(MDA)]^{2+}$ and $[Ru(NH_3)_4(MDA)_2]^{2+}$ series of complexes are 13.6 and 14.7 $cm^{-1}/10^3$, respectively (standard deviation = 400 cm^{-1} for each series). Note that we have not estimated the $E^{0'0} - h\nu_{max}(em)$ for the complexes and that these differences are estimated to run between 200 and 1000 cm^{-1};[18,44] on the basis of the apparent differences in bandwidths, they are probably larger for the $[Ru(NH_3)_5(MDA)]^{2+}$ complex than for the $[Ru(NH_3)_4(MDA)_2]^{2+}$ complex. Overall, $E(^3MC_{X(Y)})$ appears to be about 15 000 cm^{-1} and nearly independent of MDA for the ammine complexes.

The referenced ^{3}MC energies of the Ru−bpy chromophores are more scattered than those of the Ru−MDA chromophores. However, values calculated for $E(^3MC_{X(Y)})$ for $[Ru(NH_3)_4bpy]^{2+}$ and $[Ru([14]aneN_4)(bpy)]^{2+}$ are in the range of energies estimated for $[Ru(NH_3)_5(MDA)]^{2+}$ and $[Ru(NH_3)_4(MDA)_2]^{2+}$ complexes, consistent with all of them being governed mostly by distortions in the Ru−am(m)ine bonds (stretching modes). The estimated $^3MC_{X(Y)}$ excited state energies are 2000−3000 cm^{-1} larger for the $[Ru(L)_2(bpy)_2]^{m+}$ complexes in which the dominant axial distortions must involve one Ru−N(bpy) bond, and the energy of $^3MC_{X(Y)}$ is apparently about 5000−6000 cm^{-1} larger for the $[Ru(bpy)_3]^{2+}$ complex in which the excited state distortions must involve two Ru−N(bpy) bonds (note that the $[Ru(bpy)_3]^{2+}$ calculations were performed using a different suite of programs).[15,23] This suggests that the electron(dσ^*)−electron(ligand-N) repulsion that results in a 0.4−0.5 Å stretching of a single Ru−NH_3 bond is opposed by the structural linkage of the pyridyl moieties of

DOI: 10.1021/acs.inorgchem.5b01193
Inorg. Chem. 2015, 54, 8495−8508

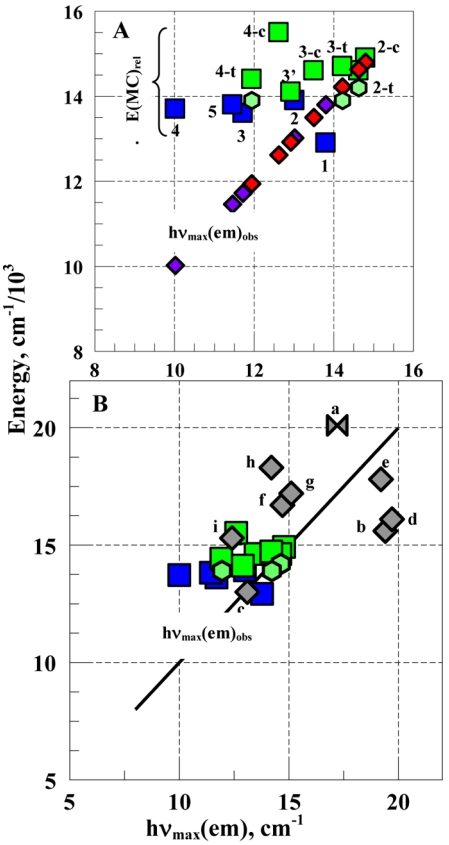

Figure 15. Comparison of the energies of the lowest energy $^3MC_{X(Y)}$ excited states to observed emission maxima. (A) $h\nu_{max}$(em), diamonds (line in panel B). Relative energies for the lowest energy ^3MC excited states: (a) squares for $MC_{X(Y)}$ states of $[Ru(NH_3)_5(MDA)]^{2+}$ (blue, respectively) and $[Ru(NH_3)_4(MDA)_2]^{2+}$ (green) and (b) hexagons for MC_z states of *trans*-$[Ru(NH_3)_4(MDA)_2]^{2+}$ complexes. The calculations were performed for the $[Ru(NH_3)_5py]^{2+}$ complex (1′), whereas the emission was obtained for its perdeutero isotopomer (1). (B) $[Ru(NH_3)_5(MDA)]^{2+}$, blue; $[Ru(NH_3)_4(MDA)_2]^{2+}$, green; $[Ru(L_4)bpy]^{m+}$, gray. The gray diamonds are for Ru−bpy chromophores with data from Thomas et al.[21] The point for $[Ru(bpy)_3]^{2+}$ is based on ^3MC calculations reported by Sun et al.,[15] and 77 K emission spectra reported by Thomas et al.[21] The code numbers in panel A are from Table 1. The code numbers in panel B indicate the complexes: a, $[Ru(bpy)_3]^{2+}$; b, $[Ru(CH_3CN)_4(bpy)]^{2+}$; c, $[Ru([14]aneN_4)(bpy)]^{2+}$; d, $[Ru([14]aneS_4)(bpy)]^{2+}$; e, $[Ru([9]aneS_3)(CN)(bpy)]^{+}$; f, $[Ru(NH_3)_2(bpy)_2]^{2+}$; g, $[Ru(en)(bpy)_2]^{2+}$; h, $[Ru(C_2O_4)(bpy)_2]$; i, $[Ru(NH_3)_4(bpy)]^{2+}$.

bpy so that the energy required to stretch the Ru−N(bpy) bond bond is larger, resulting in larger ^3MC excited state energies for the bis- and tris-bpy complexes. Thus, the higher ^3MC energies could be a stereochemical consequence of the need to stretch only one Ru−bpy bond of the bipyridine ligand. However, this comparison may also be complicated by differences in Jahn−Teller distortions for trigonal symmetry, as in $[Ru(bpy)_3]^{2+}$, and the tetragonal symmetry characteristic of most of the complexes considered here.

CONCLUSIONS

The $[Ru(NH_3)_5(MDA)]^{2+}$ complexes emit weakly but with moderate lifetimes in 77 K glasses. Except for the $[Ru(NH_3)_5(py)]^{2+}$ complex, the DFT modeling indicates that the ^3MLCT excited states of the Ru−MDA complexes have barriers to IC of more than $4k_BT$ at 77 K. Consequently, it is very unlikely, at least at 77 K, that the weak ^3MLCT emissions of many of these complexes arise from facile internal conversion to a metal-centered excited state.

The DFT modeled lowest energy ^3MC excited states of the $[Ru(NH_3)_5(MDA)]^{2+}$ complexes, other than $[Ru(NH_3)_5(py)]^{2+}$, conform well to the patterns of Jahn−Teller distortions expected in tetragonal symmetries: (1) the $d\sigma^*$ (O_h) orbital degeneracy is removed with the higher energy state distorted along the molecular Z axis (corresponding to population of a d_{z^2} orbital) and the lower energy state distorted along the X and Y axes (corresponding to population of a $d_{x^2-y^2}$ orbital) combined with (2) a pseudo-Jahn−Teller interaction that removes the X and Y axes' degeneracy. While the qualitative ordering of $E(^3MC_Z) > E(^3MC_{X(Y)})$ seems likely, the ^3MC_Z excited states have tended to be dissociative, and their energies are not meaningfully compared to those of bound states. The lower energy $^3MC_{X(Y)}$ states appear to be weakly bound, and their distortions result in a 0.4−0.5 Å lengthening (relative to the ground state) of each Ru−NH_3 bond along a H_3N−Ru−NH_3 axis.

The DFT modeling of the $[Ru(NH_3)_5(py)]^{2+}$ complex indicates that its lowest energy excited state behavior is dominated by configurational mixing between the ^3MLCT and ^3MC_z excited states. This excited state/excited state mixing results in a nearly flat PE surface along the Ru−py dissociation coordinate with very little barrier to $^3MLCT/^3MC_z$ IC. The ^3MC_z state is dissociative and leads to formation of py and a singlet $[Ru(NH_3)_5]^{2+}$ species. This contributes to both the difficulty in detecting its emission (a result of the nearly barrierless IC) and to the unusually broad emission spectrum found for its perdeutero isotopomer (due to the nearly flat PE surface along the dissociation coordinate). Furthermore, the dissociation products, py and singlet $[Ru(NH_3)_5]^{2+}$, can recombine to form a η^2(C═C) py bond to Ru, which has a large enough barrier for relaxing to the original ground state to account for the previously observed metastable intermediate.

Since the lengths of the bonds along one axis of the ^3MC states are stretched to very near to the dissociation limit, most of the Ru^{II}−ligand ground state bond energy is lost in the ^3MC excited states. Thus, the DFT modeling suggests that the energies of the ^3MC excited states must be very close to the energy required to break two coaxial Ru−ligand bonds in the ground state; for H_3N−Ru−NH_3, this is calculated to be about 19 000 cm^{-1}. Weaker bonding along the Z axis can result in $E(^3MC_Z) < E(^3MC_{X(Y)})$, as found for *trans*-$[Ru(NH_3)_4(MDA)_2]^{2+}$ complexes (the calculated bond dissociation energy is about 10% smaller for Ru−py than for Ru−NH_3). Thus, the energies of the lowest energy metal-centered excited states, $^3MC_{X(Y)}$, in the ruthenium complexes with only ammines along at least one Cartesian axis are in the range of 15 000 to 16 000 cm^{-1} and nearly independent of the acceptor ligand in the Ru−A chromophore. $E(^3MC)$ appears to increase with the Ru−L bond energy along the Cartesian axis with the weakest Ru−L bonds and with stereochemical constraints on large amplitude ligand distortions. These observations suggest a basis for selecting Ru photosensitizers with lower energy ^3MLCT than ^3MC excited states: the 77 K MLCT emission maximum of the sensitizer should have a lower energy than the energy for breaking both Ru−ligand bonds along the weakest bonding axis.

DOI: 10.1021/acs.inorgchem.5b01193
Inorg. Chem. 2015, 54, 8495−8508

■ ASSOCIATED CONTENT

Supporting Information

The Supporting Information is available free of charge on the ACS Publications website at DOI: 10.1021/acs.inorgchem.5b01193.

Electrochemistry, absorption, and emission parameters for target complexes; 77 K emission spectra of *cis*-/*trans*-$[Ru(NH_3)_4(MDA)_2]^{2+}$; correlations of absorption and emission maxima; 77 K emission spectra of Ru-bpy complexes; 77 K noisy emission spectra of the $[Ru(NH_3)_5(MDA)]^{2+}$ complexes; ambient absorption, 77 K emission, and lifetime parameters of the complexes of Ru-bpy chromophores; plot of k_{obs} vs $\Delta E(^3MLCT/^3MC)$ for Ru−MDA chromophores; table of *XYZ* coordinates for the calculated structures (PDF).

■ AUTHOR INFORMATION

Corresponding Authors

*E-mail: hbs@chem.wayne.edu (H.B.S.).
*E-mail: 054971@mail.fju.edu.tw (Y.J.C.).
*E-mail: jfe@chem.wayne.edu (J.F.E.).

Notes

The authors declare no competing financial interest.

■ ACKNOWLEDGMENTS

This work was funded in part (Y.J.C.) by the Ministry of Science and Technology (Taiwan, R.O.C) through grant no. NSC 101-2113-M-030-005 and in part (J.F.E. and H.B.S.) by the Division of Chemical Sciences, Geosciences, and Biosciences, Office of Basic Energy Sciences of the U.S. Department of Energy through grant no. DE-FG02-09ER16120. We thank Y.-H. Tian, M.-L. Yeh, and X. Z. Zhang for their efforts in multiple syntheses and purification of complexes.

■ REFERENCES

(1) Englman, R.; Jortner, J. *Mol. Phys.* **1970**, *18*, 145.
(2) Freed, K. F.; Jortner, J. *J. Chem. Phys.* **1970**, *52*, 6272.
(3) Birks, J. B. *Photophysics of Aromatic Molecules*; Wiley-Interscience: New York, 1970.
(4) Crosby, G. A. *Acc. Chem. Res.* **1975**, *8*, 231.
(5) Ulstrup, J.; Jortner, J. *J. Chem. Phys.* **1975**, *63*, 4358.
(6) Juris, A.; Balzani, V.; Barigelletti, F.; Campagna, S.; Belser, P. l.; von Zelewsky, A. *Coord. Chem. Rev.* **1988**, *84*, 85.
(7) Yersin, H.; Braun, D.; Hensler, G.; Galhuber, E. In *Vibronic Processes in Inorganic Chemistry*; Flint, C. D., Ed.; Kluwer: Dordrecht, 1989; p 195.
(8) Bixon, M.; Jortner, J.; Cortes, J.; Heitele, H.; Michel-Beyerle, M. E. *J. Phys. Chem.* **1994**, *98*, 7289.
(9) Bixon, M.; Jortner, J.; Verhoeven, J. W. *J. Am. Chem. Soc.* **1994**, *116*, 7349.
(10) Endicott, J. F.; Perkovic, M. W.; Heeg, M. J.; Ryu, C. K.; Thompson, D. In *Electron Transfer Reactions: Inorganic, Organometallic and Biological Applications*; Isied, S. S., Ed.; American Chemical Society: Washington, DC, 1997; Vol. *253*, p 199.
(11) Balzani, V.; Credi, A.; Venturi, M. *Coord. Chem. Rev.* **1998**, *171*, 3.
(12) Endicott, J. F. In *Electron Transfer in Chemistry*; Balzani, V., Ed.; Wiley-VCH: New York, 2001; Vol. *1*, p 238.
(13) Bloino, J.; Biczysko, M.; Santoro, F.; Barone, V. *J. Chem. Theory Comput.* **2010**, *6*, 1256.
(14) Wagenknecht, P. S.; Ford, P. C. *Coord. Chem. Rev.* **2011**, *255*, 591.
(15) Sun, Q.; Mosquera-Vazquez, S.; Daku, L. M. L.; Guénée, L.; Goodwin, H. A.; Vauthey, E.; Hauser, A. *J. Am. Chem. Soc.* **2013**, *135*, 13660.
(16) Durante, V. A.; Ford, P. C. *Inorg. Chem.* **1979**, *18*, 588.
(17) Malouf, G.; Ford, P. C. *J. Am. Chem. Soc.* **1977**, *99*, 7213.
(18) Lord, R. L.; Allard, M. M.; Thomas, R. A.; Odongo, O. S.; Schlegel, H. B.; Chen, Y.-J.; Endicott, J. F. *Inorg. Chem.* **2013**, *52*, 1185.
(19) Tsai, C.-N.; Tian, Y.-H.; Shi, X.; Lord, R. L.; Luo, D.-W.; Schlegel, H. B.; Endicott, J. F.; Chen, Y.-J. *Inorg. Chem.* **2013**, *52*, 9774.
(20) Mazumder, S.; Thomas, R. A.; Lord, R. L.; Schlegel, H. B.; Endicott, J. F. *Can. J. Chem.* **2014**, *92*, 996.
(21) Thomas, R. A.; Tsai, C. N.; Mazumder, S.; Lu, I. C.; Lord, R. L.; Schlegel, H. B.; Endicott, J. F.; Chen, Y. J. *J. Phys. Chem. B* **2015**, *119*, 7393.
(22) Endicott, J. F.; Ramasami, T.; Tamilarasan, R.; Lessard, R. B.; Ryu, C. K.; Brubaker, G. B. *Coord. Chem. Rev.* **1987**, *77*, 1.
(23) Sun, Q.; Mosquera-Vazquez, S.; Suffren, Y.; Hankache, J.; Amstutz, N.; Lawson Daku, L. M.; Vauthey, E.; Hauser, A. *Coord. Chem. Rev.* **2015**, *282*−*283*, 87.
(24) Frisch, M. J.; Trucks, G. W.; Schlegel, H. B.; Scuseria, G. E.; Robb, M. A.; Cheeseman, J. R.; Scalmani, G. B.; et al. *Gaussian development version*, Revision H.20; Gaussian, Inc.: Wallingford, CT, 2010.
(25) Santoro, F.; Improta, R.; Lami, A.; Bloino, J.; Barone, V. *J. Chem. Phys.* **2007**, *126*, 084509.
(26) Santoro, F.; Lami, A.; Improta, R.; Barone, V. *J. Chem. Phys.* **2007**, *126*, 184102.
(27) Santoro, F.; Lami, A.; Improta, R.; Bloino, J.; Barone, V. *J. Chem. Phys.* **2008**, *128*, 224311.
(28) Bloino, J.; Biczysko, M.; Crescenzi, O.; Barone, V. *J. Chem. Phys.* **2008**, *128*, 244105.
(29) Tu, Y.-J.; Mazumder, S.; Endicott, J. F.; Turro, C.; Kodanko, J. J.; Schlegel, H. B. *Inorg. Chem.* **2015**, DOI: 10.1021/acs.inorgchem.5b01202.
(30) Kasha, M. *Discuss. Faraday Soc.* **1950**, *9*, 14.
(31) Chang, J. P.; Fung, E. Y.; Curtis, J. C. *Inorg. Chem.* **1986**, *25*, 4233.
(32) Krentzien, H. J. Ph.D. Dissertation, Stanford University, 1976.
(33) Ford, P.; Rudd, D. F. P.; Gaunder, R.; Taube, H. *J. Am. Chem. Soc.* **1968**, *90*, 1187.
(34) Creutz, C.; Taube, H. *J. Am. Chem. Soc.* **1969**, *91*, 3988.
(35) Taube, H.; Gaunder, R. G. *Inorg. Chem.* **1970**, *9*, 2627.
(36) Allard, M. M.; Odongo, O. S.; Lee, M. M.; Chen, Y.-J.; Endicott, J. F.; Schlegel, H. B. *Inorg. Chem.* **2010**, *49*, 6840.
(37) Pavanin, L. A.; da Rocha, Z. N.; Giesbrecht, E.; Tfouni, E. *Inorg. Chem.* **1991**, *30*, 2185.
(38) Plummer, E. A.; Zink, J. I. *Inorg. Chem.* **2006**, *45*, 6556.
(39) Tfouni, E.; Ford, P. C. *Inorg. Chem.* **1980**, *19*, 72.
(40) Zwickel, A. M.; Creutz, C. *Inorg. Chem.* **1971**, *10*, 2395.
(41) Supporting Information.
(42) Curtis, J. C.; Sullivan, B. P.; Meyer, T. J. *Inorg. Chem.* **1983**, *22*, 224.
(43) Evans, I. P.; Spencer, A.; Wilkinson, G. *J. Chem. Soc., Dalton Trans.* **1973**, 204.
(44) Xie, P.; Chen, Y.-J.; Uddin, M. J.; Endicott, J. F. *J. Phys. Chem. A* **2005**, *109*, 4671.
(45) Bryant, G. M.; Fergusson, J. E.; Powell, H. K. *Aust. J. Chem.* **1971**, *24*, 257.
(46) Chen, Y.-J.; Xie, P.; Endicott, J. F.; Odongo, O. S. *J. Phys. Chem. A* **2006**, *110*, 7970.
(47) Sharma, R.; Thomas, R. A.; Tu, Y.-J.; Mazumder, S.; Alnead, M.; Schlegel, H. B.; Endicott, J. F.; Kodanko, J. J. Unpublished results, 2015
(48) Chen, Y.-J.; Xie, P.; Endicott, J. F. *J. Phys. Chem. A* **2004**, *108*, 5041.
(49) Becke, A. D. *J. Chem. Phys.* **1993**, *98*, 5648.
(50) Perdew, J. P. *Phys. Rev. B: Condens. Matter Mater. Phys.* **1986**, *33*, 8822.

DOI: 10.1021/acs.inorgchem.5b01193
Inorg. Chem. 2015, 54, 8495−8508

(51) Perdew, J. P.; Burke, K.; Wang, Y. *Phys. Rev. B: Condens. Matter Mater. Phys.* **1996**, *54*, 16533.
(52) Andrae, D.; Haussermann, U.; Dolg, M.; Stoll, H.; Preuss, H. *Theoretica Chimica Acta* **1990**, *77*, 123.
(53) Francl, M. M.; Petro, W. J.; Hehre, W. J.; Binkley, J. S.; Gordon, M. S.; DeFrees, D. J.; Pople, J. A. *J. Chem. Phys.* **1982**, *77*, 3654.
(54) Hariharan, P. C.; Pople, J. A. *Theoret. Chimica Acta* **1973**, *28*, 213.
(55) Marenich, A. V.; Cramer, C. J.; Truhlar, D. G. *J. Phys. Chem. B* **2009**, *113*, 6378.
(56) Seeger, R.; Pople, J. A. *J. Chem. Phys.* **1977**, *66*, 3045.
(57) Schlegel, H. B.; McDouall, J. J. In *Computational Advances in Organic Chemistry*; Ögretir, C., Csizmadia, I. G., Eds.; Kluwer Academic: Amsterdam, The Netherlands, 1991.
(58) Bauernschmitt, R.; Ahlrichs, R. *J. Chem. Phys.* **1996**, *104*, 9047.
(59) *Computational Advances in Organic Chemistry*; Ögretir, C., Csizmadia, I. G., Eds.; Kluwer Academic: Amsterdam, The Netherlands, 1991.
(60) Steinmann, S. N.; Piemontesi, C.; Delachat, A.; Corminboeuf, C. J. *J. Chem. Theory Comput.* **2012**, *8*, 1629.
(61) Milko, P.; Iron, M. A. *J. Chem. Theory Comput.* **2014**, *10*, 220.
(62) Pennington, R.; Keith, T.; Millam, J. M. *GaussView*; Semichem, Inc.: Shawnee Mission, KS, 2009.
(63) Kalyanasundaram, K. *Photochemistry of Polypyridine and Porphyrin Complexes*; Academic Press: New York, 1992.
(64) Balzani, V.; Juris, A.; Venturi, M.; Campagna, S.; Serroni, S. *Chem. Rev.* **1996**, *96*, 759.
(65) Endicott, J. F.; Chen, Y. J. *Coord. Chem. Rev.* **2007**, *251*, 328.
(66) Tsai, C.-N.; Endicott, J. F.; Chen, Y.-J. *Inorg. Chem.*, to be submitted.
(67) Yoshikawa, N.; Yamabe, S.; Sakaki, S.; Kanehisa, N.; Inoue, T.; Takashima, H. J. *J. Mol. Struct.* **2015**, *1094*, 98.
(68) Bersuker, I. B. *The Jahn-Teller Effect and Vibronic Interactions in Modern Chemistry*; Plenum: New York, 1984.
(69) Bersuker, I. B. *Chem. Rev.* **2013**, *113*, 1351.
(70) Tsai, C. N.; Mazumder, S.; Shi, X.; Zhang, X. Z.; Schlegel, H. B. This work.
(71) Hakamata, K.; Urushiyama, A.; Kupka, H. *J. Phys. Chem.* **1981**, *85*, 1983.
(72) Tsukerblat, B. S. *Group Theory in Chemistry and Spectroscopy*; Academic: London, 1994.
(73) Wilson, R. B.; Solomon, E. I. *J. Am. Chem. Soc.* **1980**, *102*, 4085.
(74) Dewar, M. *Bull. Soc. Chim. Fr.* **1951**, *18*, C79.
(75) Chatt, J.; Duncanson, L. A. *J. Chem. Soc.* **1953**, 2939.
(76) Chatt, J.; Duncanson, L. A.; Venanzi, L. M. *J. Chem. Soc.* **1955**, 4456.

DOI: 10.1021/acs.inorgchem.5b01193
Inorg. Chem. 2015, 54, 8495−8508